ELSEVIER

Coastal Engineering 32 (1997) 255–287

COASTAL ENGINEERING

Surf zone dynamics simulated by a Boussinesq type model. Part I. Model description and cross-shore motion of regular waves

P.A. Madsen *, O.R. Sørensen, H.A. Schäffer

International Research Centre for Computational Hydrodynamics (ICCH), Danish Hydraulic Institute, Agern Alle 5, 2970 Hørsholm, Denmark

Received 2 April 1997; revised 23 September 1997; accepted 23 September 1997

Abstract

This is the first of three papers on the modelling of various types of surf zone phenomena. In this first paper, part I, the model is presented and its basic features are studied for the case of regular waves. The model is based on two-dimensional equations of the Boussinesq type and it features improved linear dispersion characteristics, possibility of wave breaking, and a moving boundary at the shoreline. The moving shoreline is treated numerically by replacing the solid beach by a permeable beach characterized by an extremely small porosity. Run-up of nonbreaking waves is verified against the analytical solution for nonlinear shallow water waves. The inclusion of wave breaking is based on the surface roller concept for spilling breakers using a geometrical determination of the instantaneous roller thickness at each point and modelling the effect of wave breaking by an additional convective momentum term. This is a function of the local wave celerity, which is determined interactively. The model is applied to cross-shore motions of regular waves including various types of breaking on plane sloping beaches and over submerged bars. Model results comprise time series of surface elevations and the spatial variation of phase-averaged quantities such as the wave height, the crest and trough elevations, the mean water level, and the depth-averaged undertow. Comparisons with physical experiments are presented. The phase-averaged balance of the individual terms in the momentum and energy equation is determined by time-integration and quantities such as the cross-sectional roller area, the radiation stress, the energy flux and the energy dissipation are studied and discussed with reference to conventional phase-averaged wave models. The companion papers present cross-shore motions of breaking

* Corresponding author. Fax: +45-45762567; e-mail: icch@dhi.dk.

PII S0378-3839(97)00028-8

irregular waves, swash oscillations and surf beats (part II) and nearshore circulations induced by breaking of unidirectional and multidirectional waves (part III). © 1997 Elsevier Science B.V.

Keywords: Boussinesq model; Wave breaking; Surf zone; Energy equation

1. Introduction

The classical method of describing wave transformation in the surf zone is based on the phase-averaged approach, in which the depth-integrated momentum and energy equations are time-averaged over a wave period and solved with respect to the spatial variation of the wave height, the setup and the wave-induced current. Important quantities such as the wave celerity, the radiation stress and the energy flux are modelled by the use of sinusoidal theory or more advanced theories such as the stream function theory. The energy dissipation is modelled by empirical relations e.g. based on the hydraulic jump analogy or the surface roller concept. Numerous examples of such models are given in the literature, for a review see e.g. Battjes (1988) and Hamm et al. (1993). More recent contributions include Dally and Brown (1995) and Lippmann et al. (1996).

A more detailed description of the nonlinear interaction processes in the surf zone requires phase-resolving models, formulated either in the time domain in terms of mass and momentum equations or in the frequency domain in terms of evolution equations.

The first examples of time domain models to be used in the surf zone, were based on the nonlinear shallow water (NSW) equations combined with a special treatment of bores and shocks: Hibberd and Peregrine (1979) used a dissipative Lax–Wendroff scheme to study run-up of regular bores, while e.g. Kobayashi et al. (1989) and Watson and Peregrine (1992) used more advanced shock-capturing methods to study swash oscillations due to regular and irregular wave trains. Due to the absence of frequency dispersion the NSW formulation is restricted to very shallow water and to the propagation of bores in the inner surf zone after wave breaking has fully developed.

The Boussinesq equations are an attractive alternative to the NSW equations, as they incorporate frequency dispersion and can be applied to a much wider wave spectrum and a larger part of the coastal region (see Freilich and Guza, 1984; Elgar et al., 1990; and others). In contrast to the NSW equations, the Boussinesq equations do not automatically lead to wave breaking in shallow water, because the frequency dispersion will tend to balance the amplitude dispersion and to stabilize the wave profiles. For this reason an extension of these equations to include the surf zone requires the introduction of breaking criteria and dissipation mechanisms.

Frequency domain formulations of the Boussinesq equations have been presented by e.g. Freilich and Guza (1984) and Madsen and Sørensen (1993) for nonbreaking waves and extended to the surf zone by Mase and Kirby (1992), Kaihatu and Kirby (1995) and Eldeberky and Battjes (1996). The key problem in these formulations is the spectral distribution of energy dissipation, which Eldeberky and Battjes assumed to be in proportion to the energy level at each frequency, while Mase and Kirby weighted the dissipation towards high frequencies through a frequency squared dependence.

Time domain formulations of Boussinesq type equations operate directly on wave profiles, and surf zone models have been obtained in a number of ways: The eddy viscosity concept related to horizontal gradients in the depth-averaged velocity (Tao, 1983; Abbott et al., 1983; Sato et al., 1991; Karambas and Koutitas, 1992), the frictional concept proportional to the depth-averaged velocity (Sato et al., 1991), the roller concept accounted for by an additional pressure term in the momentum equations (Deigaard, 1989; Brocchini et al., 1992), and the roller concept resulting in an additional convective momentum term (Schäffer et al., 1993).

The present work is based on the time domain formulation by Schäffer et al. (1993), which is extended in a number of ways: Firstly, the formulation is generalized to two horizontal dimensions. Secondly, the underlying Boussinesq equations are chosen to incorporate improved accuracy of linear dispersion and nonlinear energy transfer. Thirdly, the model is extended to the swash zone by including a numerical treatment of the moving shoreline. Finally, an interactive determination of the wave celerity is introduced, which is important for the case of irregular waves and for the interaction of short and long waves in the swash zone.

The objective of this series of papers (parts I–III) is to study a number of surf zone and swash zone phenomena. The phenomena to be studied include the transformation, breaking and decay of regular and irregular wave trains, the resulting run-up and swash oscillations and the generation of surf beats and wave induced circulations. In addition to the wave breaking mechanism, some of the key phenomena to be studied will be triad interactions in general, with special emphasis on the interaction between short and long waves. In part I we shall present the numerical model and concentrate on cross-shore motions of regular waves. The regular wave examples and the analyses of wave-averaged quantities are chosen in order to establish the link to traditional phase-averaged models. The real strength of the model lies in its applicability to more complex physical phenomena as pursued in parts II and III of this work. Part II (Madsen et al., 1997) concentrates on cross-shore motions of irregular waves, swash oscillations and surf beat, while part III (Sørensen et al., 1998) deals with two-dimensional situations with a detached breakwater and a rip-channel, respectively, including nearshore circulations induced by irregular multidirectional breaking waves.

This paper is organized as follows: The formulation of the numerical model is given in Section 2. In Section 3 the model is applied to various types of wave breaking on plane sloping beaches and over submerged bars. In Section 4 we concentrate on a number of phase-averaged quantities such as the undertow, the roller area, the radiation stress and the energy flux, which play an important role in conventional phase-averaged momentum and energy equations. The net energy dissipation resulting from the present modified Boussinesq equations is determined and compared to explicit expressions from the literature. Section 3 and Section 4 further include a comparison with data from various laboratory experiments.

2. Formulation of the numerical model

The numerical model is based on two-dimensional equations of the Boussinesq type using a flux-formulation with improved linear dispersion characteristics. The model is

extended to include the possibility of wave breaking of regular and irregular waves in two horizontal dimensions and to take into account a moving shoreline allowing for a study of the surf zone and swash zone.

The incorporation of wave breaking in the two-dimensional Boussinesq model is based on the concept of surface rollers. We shall outline the roller model in the following and analyze it in further detail in Section 4. The breaking procedure can be split up into four parts:

- The effect of the roller on the wave motion (Section 2.1).
- The position of the break point (Section 2.2).
- The geometrical determination of the roller (Section 2.3).
- The determination of the roller celerity (Section 2.4).

Finally, the moving shoreline is treated numerically by replacing the solid beach by a permeable beach characterized by an extremely small porosity. This technique is described in Section 2.5, which also includes a verification of the procedure on run-up of nonbreaking waves.

2.1. Basic equations including a model for wave breaking

The determination of the effect of the surface rollers on the wave motion is inspired by the simple model suggested by Svendsen (1984a). The basic principle is that the surface roller is considered as a volume of water being carried by the wave with the wave celerity and this is assumed to result in the vertical distribution of the horizontal particle velocity shown in Fig. 1. By assuming this velocity profile to be valid in case of wave breaking, the following modified version of the Boussinesq equations appears

$$\frac{\partial \eta}{\partial t} + \frac{\partial P}{\partial x} + \frac{\partial Q}{\partial y} = 0 \tag{2.1a}$$

$$\frac{\partial P}{\partial t} + \frac{\partial}{\partial x}\left(\frac{P^2}{d}\right) + \frac{\partial}{\partial y}\left(\frac{PQ}{d}\right) + \frac{\partial R_{xx}}{\partial x} + \frac{\partial R_{xy}}{\partial y} + gd\frac{\partial \eta}{\partial x} + \psi_x + \frac{\tau_x}{\rho} = 0 \tag{2.1b}$$

$$\frac{\partial Q}{\partial t} + \frac{\partial}{\partial y}\left(\frac{Q^2}{d}\right) + \frac{\partial}{\partial x}\left(\frac{PQ}{d}\right) + \frac{\partial R_{yy}}{\partial y} + \frac{\partial R_{xy}}{\partial x} + gd\frac{\partial \eta}{\partial y} + \psi_y + \frac{\tau_y}{\rho} = 0 \tag{2.1c}$$

Here (P, Q) is the depth integrated velocity (the volume flux) in the Cartesian

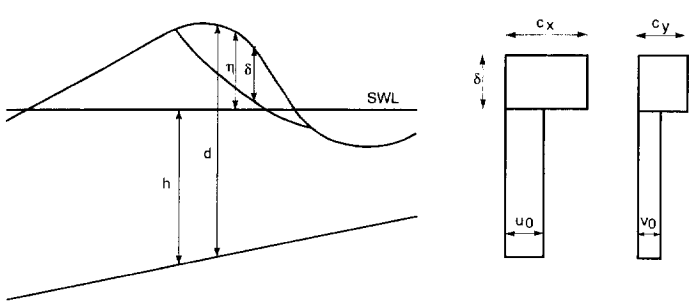

Fig. 1. Definition sketch: Cross-section of a breaking wave and assumed vertical profile of the horizontal particle velocity components.

coordinate system $(x,\ y)$, $d = h + \eta$ is the instantaneous depth and η is the surface elevation.

The terms denoted R_{xx}, R_{xy} and R_{yy} account for the excess momentum originating from the nonuniform velocity distribution due to the presence of the roller and they are defined by

$$(R_{xx},\ R_{xy},\ R_{yy}) \equiv \frac{\delta}{1-\delta/d}\left(\left(c_x - \frac{P}{d}\right)^2,\ \left(c_x - \frac{P}{d}\right)\left(c_y - \frac{Q}{d}\right),\ \left(c_y - \frac{Q}{d}\right)^2\right) \tag{2.2}$$

This is a two-dimensional generalization of the formulation by Schäffer et al. (1993). Here $\delta = \delta(t,\ x,\ y)$ is the thickness of the surface roller and $(c_x,\ c_y)$ are the components of the roller celerity. The determination of these quantities is described in Sections 2.3 and 2.4. In Section 4 we shall analyze in detail the effect of introducing these terms and determine the resulting energy loss.

The terms denoted ψ_x and ψ_y are dispersive Boussinesq type terms which in shallow water may be taken from Peregrine (1967). Here we use the formulation derived under the mild-slope assumption by Madsen and Sørensen (1992) providing improved frequency dispersion:

$$\psi_x \equiv -\left(B+\frac{1}{3}\right)h^2\left(\frac{\partial^3 P}{\partial x^2\partial t} + \frac{\partial^3 Q}{\partial x\partial y\partial t}\right) - Bgh^3\left(\frac{\partial^3\eta}{\partial x^3} + \frac{\partial^3\eta}{\partial x\partial y^2}\right) - h\frac{\partial h}{\partial x}\left(\frac{1}{3}\frac{\partial^2 P}{\partial x\partial t} + \frac{1}{6}\frac{\partial^2 Q}{\partial y\partial t} + 2Bgh\frac{\partial^2\eta}{\partial x^2} + Bgh\frac{\partial^2\eta}{\partial y^2}\right) - h\frac{\partial h}{\partial y}\left(\frac{1}{6}\frac{\partial^2 Q}{\partial x\partial t} + Bgh\frac{\partial^2\eta}{\partial x\partial y}\right) \tag{2.3a}$$

$$\psi_y \equiv -\left(B+\frac{1}{3}\right)h^2\left(\frac{\partial^3 Q}{\partial y^2\partial t} + \frac{\partial^3 P}{\partial x\partial y\partial t}\right) - Bgh^3\left(\frac{\partial^3\eta}{\partial y^3} + \frac{\partial^3\eta}{\partial x^2\partial y}\right) - h\frac{\partial h}{\partial y}\left(\frac{1}{3}\frac{\partial^2 Q}{\partial y\partial t} + \frac{1}{6}\frac{\partial^2 P}{\partial x\partial t} + Bgh\frac{\partial^2\eta}{\partial x^2} + 2Bgh\frac{\partial^2\eta}{\partial y^2}\right) - h\frac{\partial h}{\partial x}\left(\frac{1}{6}\frac{\partial^2 P}{\partial y\partial t} + Bgh\frac{\partial^2\eta}{\partial x\partial y}\right) \tag{2.3b}$$

The dispersion coefficient, B is set to the value $1/15$, which provides linear dispersion characteristics corresponding to a Padé [2,2] expansion of the Stokes linear dispersion relation.

Finally, bottom friction is included in the formulation of (Eq. (2.1b)) and (Eq. (2.1c)) by the terms τ_x/ρ and τ_y/ρ. In part I bottom friction will be neglected as it is insignificant for the cross-shore applications studied here.

2.2. Determination of the break point

Incipient breaking is assumed to occur when the local slope of the surface elevation exceeds an initial critical value, $\tan\phi_B$ as suggested by Deigaard (1989). For a number of test cases with spilling breakers on plane sloping beaches Schäffer et al. (1993) found that acceptable results could be obtained by using the universal value $\phi_B = 20$ deg. Also in the present work we shall use this value as our default breaking criterion, although we

realize that it will probably not be generally applicable for other types of breaking. We shall investigate this in further detail in Section 3, where e.g. two cases of plunging breakers are considered and other values of ϕ_B are tested.

The calibration of ϕ_B is obviously closely related to the accuracy of the computed surface elevations before breaking occurs and unfortunately this is one of the weak points in conventional Boussinesq models: While the Boussinesq terms given by (Eqs. (2.3a) and (2.3b)) provide excellent linear shoaling characteristics for kh (wave number times depth) as large as 3 (see Madsen and Sørensen, 1992), the transfer of energy to super-harmonics is generally underestimated e.g. the second harmonic is underestimated with more than 10% for kh larger than 0.5 (see Madsen and Sørensen, 1993). As nonlinear shoaling is a combination of linear shoaling characteristics and nonlinear transfer to higher harmonics the combination of the two mechanisms result in underestimated wave heights and crest elevations near the breaking point. This general conclusion is supported by the simulations presented in Section 3.

It should also be emphasized that in contrast to the present flux formulation, a velocity formulation of the standard Boussinesq equations will typically lead to overestimated higher harmonics (at least for small wave numbers) and a general improvement of nonlinear shoaling requires a higher order formulation of the equations. Transfer functions for a variety of lower and higher order Boussinesq type equations can be found in Madsen and Schäffer (1997).

For the above reasons the present model can be expected to underestimate nonlinearity and wave heights in the vicinity of the break point, and consequently the chosen or calibrated breaker angle ϕ_B would typically be smaller than values observed in laboratory experiments. It is expected that a future model based on a combination of the roller concept and higher order equations will require a revision of ϕ_B.

2.3. Determination of the surface rollers

The temporal and spatial determination of the rollers is based on a heuristic, geometrical approach as described in detail by Schäffer et al. (1993). Due to the transition from initial breaking to a bore-like stage in the inner surf zone, the critical angle, ϕ, is assumed to gradually change from ϕ_B to a smaller terminal angle ϕ_0. Hence the instantaneous value of ϕ will depend on the age of the roller and is assumed to follow an exponential time-variation,

$$\tan\phi(t) = \tan\phi_0 + (\tan\phi_B - \tan\phi_0)\exp\left[-\ln 2\frac{t-t_B}{t_{1/2}}\right], \tag{2.4}$$

where $t_{1/2}$ defines the time scale for the development of the roller and t_B is the time of incipient breaking. Locally, the roller is defined as the water above the tangent of slope $\tan\phi$ and wave breaking is assumed to cease when the maximum of the local slope becomes less than $\tan\phi$. After the determination of the roller at each time step, the roller thickness, δ, is multiplied by a shape factor f_δ prior to the inclusion in the governing equations. In two horizontal dimensions the toe of the roller becomes a curve instead of a single point and the tangent becomes a set of generating lines determined by the instantaneous local angle $\phi(t)$. Whereas $\phi(t)$ in the one-dimensional case is constant within each roller, it is allowed to have a lateral variation in the two-dimen-

sional case. This makes the detection of rollers more complicated and we shall return to a detailed discussion of this problem in the companion paper, part III.

One disadvantage of the heuristic determination of surface rollers is that in addition to ϕ_B, it relies on three parameters ϕ_0, $t_{1/2}$ and f_δ. We have tested the effect of varying each of these parameters and have obtained the following experience:

Firstly, the value of ϕ_0 is not critical for applications, where breaking continues all the way to the shoreline. A small decrease of ϕ_0 will have almost no effect on the evolution of the roller area except for a moderate increase in the maximum value which again leads to a larger energy dissipation and a slightly steeper wave height decay. Based on the analogy to the hydraulic jump, Deigaard (1989) estimated ϕ_0 to be of the order 10 deg and this choice is used as the default value in our calculations. However, in a special case of breaking over a horizontal part of a submerged bar (studied in Section 3.2), reasonable agreement with laboratory experiments requires that ϕ_0 is reduced to 7–8 deg in combination with a similar reduction of ϕ_B.

Secondly, the parameter $t_{1/2}$ defines the transition between the two breaker angles and we have tested the influence of varying it in the interval $T/10$ to $T/2$, where T is a characteristic period of the incident wave train. An increase of $t_{1/2}$ effects the roller area in two ways: The maximum value is reduced and the initial growth becomes smaller. This results in a slightly milder decay of the wave height. We use the value $T/5$ as the default value in our calculations.

Thirdly, the parameter f_δ has been varied in the interval from 1.0 to 2.0. It turns out that although a large f_δ gives a large roller in the instantaneous determination, the wave averaged effect is weak. One explanation for this is, that an effort to enlarge the roller (imposing a large f_δ) results in an increasing dissipation tending to reduce the roller size in the time steps to follow. We have fixed f_δ to the value of 1.5 in all calculations presented here.

In order to quantify the model as a predictive tool, all test cases (in parts I–III) are modelled with the default parameter set $(\phi_B, \phi_0, t_{1/2}, f_\delta) = (20 \text{ deg}, 10 \text{ deg}, T/5, 1.5)$. In addition, some test cases are shown with other sets of breaker parameters.

2.4. Determination of wave celerity

The wave celerity, which is assumed to be identical to the roller velocity is an essential parameter in the roller model. In previous publications such as Schäffer et al. (1993) we have used the approximation $c = 1.3\sqrt{gh}$, where h is the still water depth, and this simple formulation works quite well for the case of regular waves, except in the swash zone. However, for wave groups and irregular waves this simple approximation is inadequate as it fails to incorporate e.g. the interaction between short and long waves in the surf zone and swash zone.

The new approach adopted here is to determine c interactively from the instantaneous wave field. Locally, we assume that the surface elevation can be expressed by $\eta = \eta(\omega t - k_x x - k_y y)$ corresponding to a regular, progressive wave field. By definition

$$(c_x, c_y) \equiv (k_x, k_y)\frac{\omega}{k^2}, \tag{2.5}$$

where k is the wave number, ω is the angular frequency and the subscripts denote x- and y-components. In terms of the surface elevation this can be expressed as

$$\begin{pmatrix} c_x \\ c_y \end{pmatrix} = \begin{pmatrix} \partial\eta/\partial x \\ \partial\eta/\partial y \end{pmatrix} \frac{-\partial\eta/\partial t}{(\partial\eta/\partial x)^2 + (\partial\eta/\partial y)^2}, \tag{2.6}$$

which we apply locally at the steepest point of each wave front. Thus, in a wave-following manner, this method provides a well-defined value of the celerity for irregular waves as well as for regular waves. In principle Eq. (2.6) only applies for progressive waves but it turns out to be a good local approximation as long as reflections of the primary waves are small.

A general problem with any interactive determination of the wave celerity is, that the feedback to the mass and momentum equations through the roller model makes it a recursive system and instabilities may occur in this process. Noise may occur in connection with the use of Eq. (2.6), which is therefore low pass filtered using a second order recursive filter.

An obvious alternative to Eq. (2.6) would be to determine c simply from the trajectories of characteristic points such as the toe of the roller or the steepest point of the wave. Such options have been tried without success, the main problem being that any trajectory can only be determined with a limited accuracy even with a subgrid representation. Hence a direct time-differentiation of this trajectory inevitably leads to very noisy solutions.

In Fig. 2 we consider regular waves breaking on a plane sloping beach with a slope of 1/40. The wave period is 1.79 s and the incoming wave height is 0.145 m in a depth of 0.70 m. The measured celerity presented by Stive (1984) is shown as a reference. In addition to the celerity computed from Eq. (2.6), Fig. 2 also shows the theoretical celerities determined by Stokes linear theory and by $c = \sqrt{gh}$ and $c = 1.3\sqrt{gh}$. Outside the surf zone the computed celerity follows Stokes theory quite closely at least as long

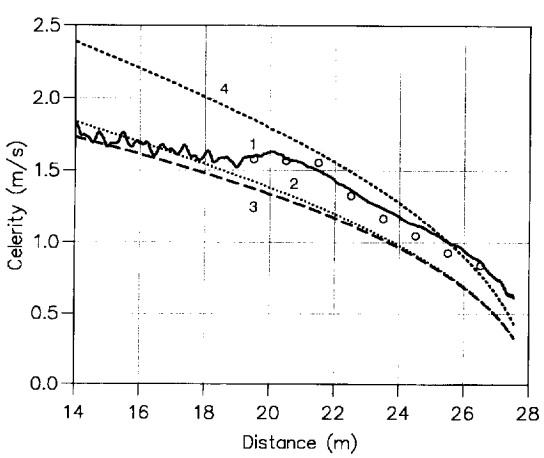

Fig. 2. Spatial variation of the wave celerity for the test of Stive (1980). (1) celerity determined interactively. (2) Celerity using Stokes linear theory. (3) $c = \sqrt{gh}$. (4) $c = 1.3\sqrt{gh}$. (○) Experimental data.

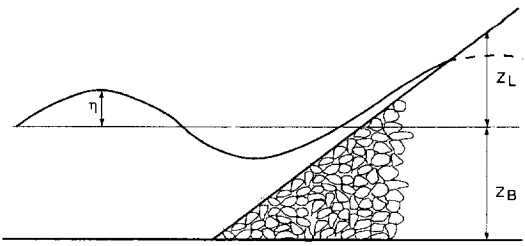

Fig. 3. Definition sketch of a beach incl. an artificial porous flow regime.

as the wave is fairly linear. In this region the computed celerity is seen to oscillate, which is due to small reflections from the breaker line. Near the break point the computed celerity exceeds the linear celerity which is to be expected because of amplitude dispersion and inside the surf zone the agreement with the measurements is excellent.

Notice also that the simple approximation of $c = 1.3\sqrt{gh}$ is fairly good inside the surf zone. This approximation is, however, not valid for bichromatic or irregular waves in which case features like the deceleration of primary waves due to downrush of long waves in the swash zone become important. Such features are automatically incorporated by the new method based on Eq. (2.6) as will be further investigated in the companion paper, part II.

2.5. Modelling a moving shoreline

One of the difficult points in simulating run-up of regular and irregular waves is the numerical treatment of the moving shoreline. In the present work we take the following approach: The computational domain is extended artificially by replacing the solid beach by a permeable beach characterized by a very small porosity. Near the moving shoreline the water surface will intersect with the sea bed and continue into the porous beach. Hence the instantaneous position of the shoreline is simply determined by this intersection (Fig. 3).

Each vertical cross-section comprises a physical regime with clear water on top of an artificial porous flow regime. The idealized vertical variation of the porosity will be unity in the physical flow regime and $\epsilon (\ll 1)$ in the porous regime below. In order to avoid numerical instabilities it is necessary to introduce a transition between the two regimes. Hence, using an exponential transition we assume the following vertical variation of the porosity

$$\gamma(z) = \begin{cases} 1, & Z_L \le z \\ \epsilon + (1-\epsilon)e^{\beta(z-Z_L)/(Z_L-Z_B)}, & Z_B \le z \le Z_L \end{cases}, \tag{2.7}$$

where $\gamma(z)$ is the porosity, ϵ is the minimum value of γ, β is a constant shape factor defining the exponential transition between the two flow regimes, z is the vertical coordinate, $\eta(x, y, t)$ is the surface elevation, $Z_L(x, y)$ defines the physical sea bed and Z_B defines the lower limit of the porous region, which should at least cover the swash

zone. In practise, Z_B is normally chosen as the datum at the toe of the slope. The variation of $\gamma(z)$ is shown in Fig. 4 (using $\beta = 100$ and $\epsilon = 0.01$), and it can be compared to the reference value of unity in clear water and zero in the porous regime. Notice that only 10% of the porous regime is included in the figure.

In principle, ϵ should be as small as possible and β as large as possible in order to avoid a distortion of the mass balance and a disturbance of the flow in the physical domain. On the other hand, the numerical solution becomes unstable for extreme values of the two parameters. In practise, it turns out that ϵ should be chosen in the interval of 0.01 to 0.001 and β of the order 100. We shall return to the determination of these parameters later in this section.

Having specified the vertical variation of the porosity, it is straightforward to determine the resulting effective water depth by integration

$$A(x, y, t) \equiv \int_{Z_B}^{\eta} \gamma(z)\mathrm{d}z \tag{2.8}$$

This effective water depth will generally replace the physical water depth in the depth-integrated momentum equations i.e.

$$\frac{\partial P}{\partial t} + \frac{\partial}{\partial x}\left(\frac{P^2}{A}\right) + \frac{\partial}{\partial y}\left(\frac{PQ}{A}\right) + gA\frac{\partial \eta}{\partial x} + \ldots = 0 \tag{2.9a}$$

$$\frac{\partial Q}{\partial t} + \frac{\partial}{\partial y}\left(\frac{Q^2}{A}\right) + \frac{\partial}{\partial x}\left(\frac{PQ}{A}\right) + gA\frac{\partial \eta}{\partial y} + \ldots = 0 \tag{2.9b}$$

The remaining question is how to determine a representative porosity, α to be used in the depth-integrated continuity equation

$$\alpha\frac{\partial \eta}{\partial t} + \frac{\partial P}{\partial x} + \frac{\partial Q}{\partial y} = 0 \tag{2.10}$$

Because of the mixture of a physical regime with clear water on top of an artificial regime with a very low porosity, one can not use the obvious choice of a depth-averaged porosity, which would lead to porous flow conditions everywhere. Instead we use

$$\alpha(x, y, t) \equiv \gamma(\eta) \tag{2.11}$$

Hence, α is a function of the local surface elevation, and it is unity in clear water and

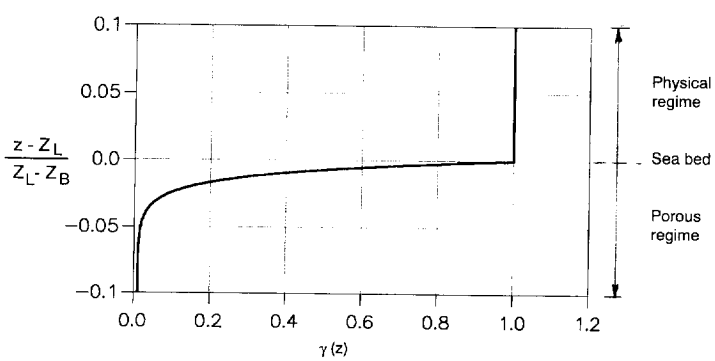

Fig. 4. Vertical variation of the porosity, $\gamma(z)$.

decays exponentially to the value of ϵ whenever the water surface disappears into the porous beach.

The description given so far in principle defines the numerical technique for handling the moving shoreline. However, in order to make this technique operational in connection with Boussinesq type models a couple of problems call for special attention: Firstly, the Boussinesq terms are switched off at the still water shoreline, where their relative importance is extremely small anyway. Hence in this region the equations simplify to the nonlinear shallow water equations. Secondly, an explicit filter is introduced near the still water shoreline to remove short-wave instabilities during uprush and downrush and to dissipate the wave energy in the area where the surface roller can not be resolved.

One of the advantages of the present method is that it is quite easy to implement and apply in two horizontal dimensions. The drawback is that the method will always introduce minor errors in the mass balance and these will generally lead to an underestimation of the maximum uprush and downrush on impermeable slopes. In situations with a very rapid variation in the shoreline motion stability problems may occur.

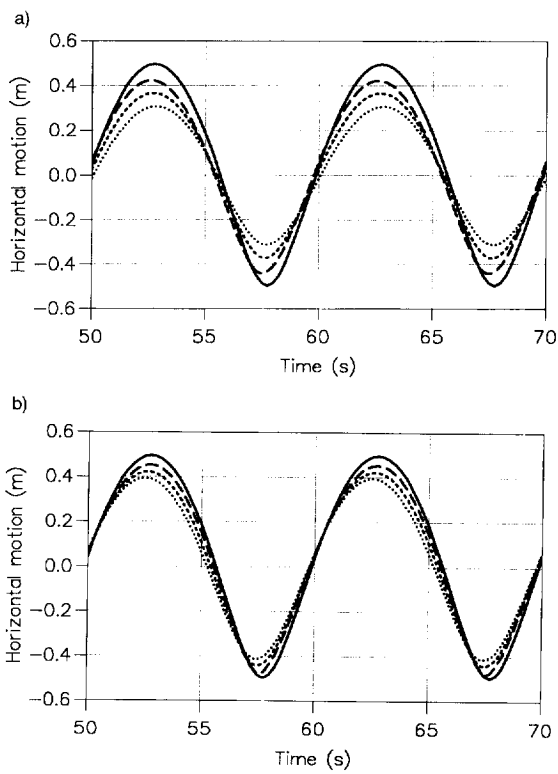

Fig. 5. Horizontal motion of the shoreline. Analytical solution (————) by Carrier and Greenspan (1958). (a) Present model with $\epsilon = 0.005$ and (1) (· · ·) $\beta = 20$; (2) (- - -) $\beta = 30$; (3) (– – –) $\beta = 100$. (b) Present model with $\beta = 100$ and (1) (· · ·) $\epsilon = 0.01$; (2) (- - -) $\epsilon = 0.005$; (3) (– – –) $\epsilon = 0.001$.

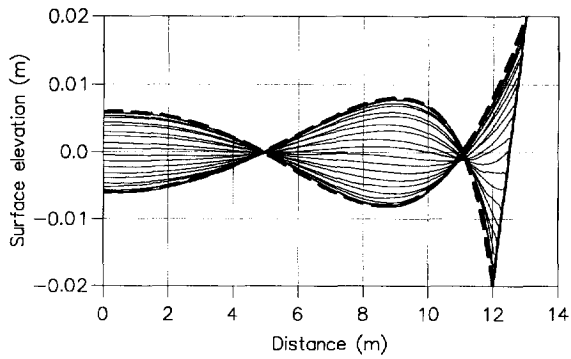

Fig. 6. Envelope of surface elevations. Analytical solution by Carrier and Greenspan (1958) (---); Present model with $\epsilon = 0.001$ and $\beta = 100$ (————).

In the following we shall verify the accuracy of the method against the analytical solution by Carrier and Greenspan (1958) for nonbreaking shallow water waves on a sloping beach. Since the analytical solution is based on the nonlinear shallow water equations, we have switched off the Boussinesq terms everywhere for this comparison. The test case considered has an initial water depth of 0.5 m, a wave period of 10 s, a slope of 1/25, and a wave height of 50% of the value giving breaking at run-down (this corresponds to an incident wave height of 0.006 m at 0.5 m depth). Fig. 5a shows the horizontal motion of the shoreline computed with a constant value of $\epsilon = 0.005$ and three different values of $\beta = 20$, 30 and 100. The full line gives the analytical result. Obviously, the numerical solution is quite sensitive to the value of β but converges towards the analytical solution for increasing β values. In Fig. 5b the value of β is kept constant $\beta = 100$ while three different ϵ values have been considered (0.01, 0.005 and 0.001). Again, the numerical solution is clearly converging towards the analytical solution, but even for an ϵ value of 0.001 the maximum run-up is still underestimated by 8%. The reason is that the upper part of the swash zone is containing only a thin film of water and this is quite sensitive to even small portions of water entering the porous beach. However, this is unimportant for the rest of the solution as can be seen more clearly from Fig. 6, showing the envelope of surface elevations. The numerical solution is obtained for the choice of $\epsilon = 0.001$ and $\beta = 100$ and the overall agreement with the analytical solution is most satisfactory.

3. Shoaling and breaking of regular waves

In this chapter the applicability of the breaker model is tested on wave breaking over gently sloping plane beaches and on wave breaking over submerged bars. The study concentrates on shoaling of unidirectional regular waves and spilling as well as plunging type of breaking is considered. The numerical model is compared with measurements from 8 laboratory experiments representing a range of different wave conditions (see Table 1). These are characterized in terms of h/L_0, H_0/L_0 and ζ, where L_0 is the deep

Table 1
List of experiments with regular waves

REFERENCE	Case	T (s)	H (m)	h/L_0	H_0/L_0	ζ
Stive (1980)	1	1.79	0.145	0.14	0.032	0.14
Hansen and Svendsen (1984)	2	2.0	0.120	0.058	0.019	0.21
Ting and Kirby (1994)	3	5.0	0.125	0.010	0.002	0.60
Luth et al. (1993)	4	1.8	0.30	0.16	0.065	0.20
Beji and Battjes (1993)	5	2.5	0.033	0.041	0.0034	s
	6	2.5	0.041	0.041	0.0042	p
	7	1.0	0.052	0.26	0.033	s
	8	1.0	0.064	0.26	0.041	p

water wave length, H_0 is an estimate of the deep water wave height, h is the water depth at the wave generator and ζ is the surf similarity parameter defined as the beach slope divided by the square root of the deep water wave steepness. Based on Galvin (1968) classification of wave breaking, Battjes (1974) found that spilling breakers would occur for $\zeta < 0.5$, while plunging would occur for $0.5 < \zeta < 3.3$.

In all numerical simulations the moving shoreline is treated as described in Section 2.5 (with $\epsilon = 0.005$ and $\beta = 100$), while the seaward boundary is treated as nonreflective using the sponge layer technique described by Larsen and Dancy (1983). Waves are generated at internal points by source terms representing the volume flux in progressive waves. For all the test cases a grid spacing of $\Delta x = 0.05$ m and a time step of $\Delta t = 0.02$ s is used. With respect to the parameters of the breaker model the following standard values are applied when nothing else is specified: $\phi_B = 20$ deg, $\phi_0 = 10$ deg, $t_{1/2} = T/5$ and $f_\delta = 1.5$.

3.1. Breaking on a gently sloping beach

Wave breaking on a gently sloping plane beach is an obvious starting point for any testing of a breaking model. Stive (1980) presented experimental results for monochromatic waves breaking on a plane slope of 1/40, a depth of 0.70 m in the horizontal part of the flume, a wave period of 1.79 s and an incoming wave height of 0.145 m. This gives a typical spilling breaker, see case 1 in Table 1. A second order Stokes wave is used as input at the toe of the slope. Fig. 7 shows the spatial variation of the wave height and the setup obtained by the measurements (circles) and by the model (full line). The overall agreement is seen to be fairly good but there are some discrepancies: The last part of the shoaling before breaking is under-estimated and the predicted break point is half a meter off in the offshore direction. Furthermore, the measured wave height decay just after breaking is clearly steeper than the computed one indicating a stronger initial energy dissipation. With a slightly higher breaker angle ($\phi_B \approx 22$ deg, not shown) the predicted position of the break point can be corrected from 19.0 m to 19.5 m as measured, but this does not improve the overall agreement. The well known horizontal shift between the break point and the point where setup starts is clearly seen in the measurements. This feature is captured by the model and it may be explained as a result

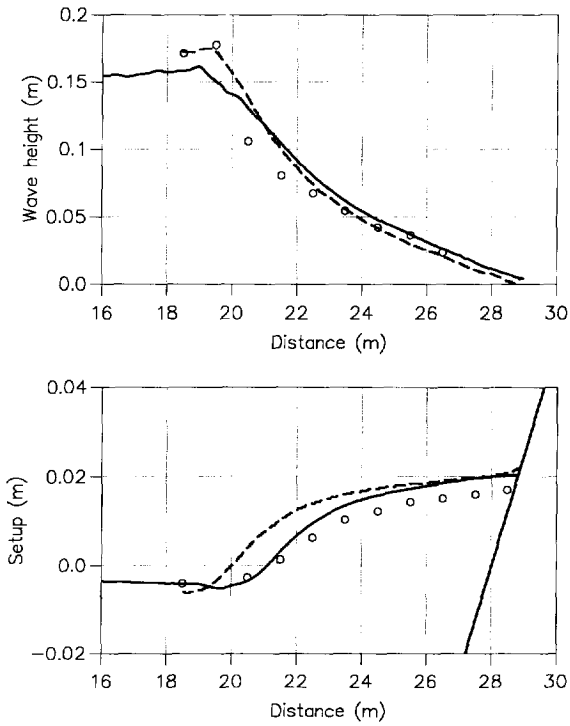

Fig. 7. Spatial variation of wave height and setup for the test of Stive (1980). Present model (————); numerical solution by Kobayashi et al. (1989) (- - -); experimental data (○).

of initial conversion of potential energy into forward momentum flux. We shall discuss this mechanism in further detail in Section 4. Fig. 7 also shows the numerical results by Kobayashi et al. (1989), who solved the nonlinear shallow water equations (NSW) by using a dissipative shock-capturing method in which bores or shock fronts are frozen to cover only a few grid points. For steep waves a NSW model will predict breaking to occur very near to the seaward boundary due to the lack of frequency dispersion. For this reason the NSW calculations were started close to the observed break point at a depth of 0.2375 m with an incoming wave height of 0.172 m. Fig. 7 shows that the overall performance of the NSW model is good except that the positions of the break point and the start of setup coincide.

As the next test case we consider the flume experiment by Hansen and Svendsen (1984) and Svendsen et al. (1987), who presented results for the wave height, setup and undertow. They used a slope of 1/34.25 with a depth of 0.36 m in the horizontal section of the flume, a wave period of 2.0 s and an incoming wave height of 0.12 m i.e. a spilling breaker in shallow water (case 2, Table 1). The Boussinesq model is started 2.7 m offshore the toe of the slope (15 m from the shoreline) using a conoidal input. The computed spatial variation of the wave height and the setup is shown in Fig. 8 in comparison with the measurements. The pronounced shoaling just up to the break point

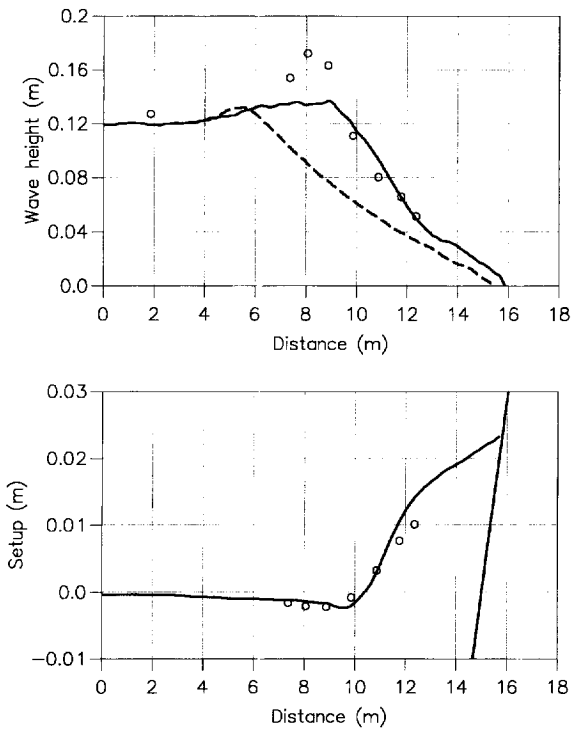

Fig. 8. Spatial variation of wave height and setup for the test of Hansen and Svendsen (1984). Present model (————); numerical solution by Kobayashi et al. (1989) (- - -); experimental data (○).

is clearly reproduced rather poorly by the model (for the reasons discussed in Section 2.2), while the position of the break point is well predicted using $\phi_B = 20$ deg. It is evident that in a model with better nonlinear shoaling characteristics than the present one, the optimal value of ϕ_B would have to be higher. Nevertheless, except for the discrepancies in the vicinity of the break point, the present model leads to a fairly good prediction of the surf zone variations of the wave height and setup. The agreement in Fig. 8 is seen to be much improved as compared with the NSW results by Kobayashi et al. (1989), who started the calculations near the toe of the slope. However, this position being quite far from the break point makes it a very difficult test for the NSW model, which fails to predict the break point and starts the decay of the wave height much too early. This test case will be studied in further detail in Section 4.

Ting and Kirby (1994) presented measurements for plunging breakers on a slope of 1/35 with an initial depth of 0.40 m, and with regular waves being generated with a wave period of 5.0 s and a wave height of 0.125 m (case 3, Table 1). Although the present breaker model is not designed to handle plunging breakers a fairly successful result can be obtained even with standard breaker parameters. The spatial variations of the crest and trough elevations and of the mean water level are shown in Fig. 9, with full lines corresponding to computations with standard parameters. We notice that the trough

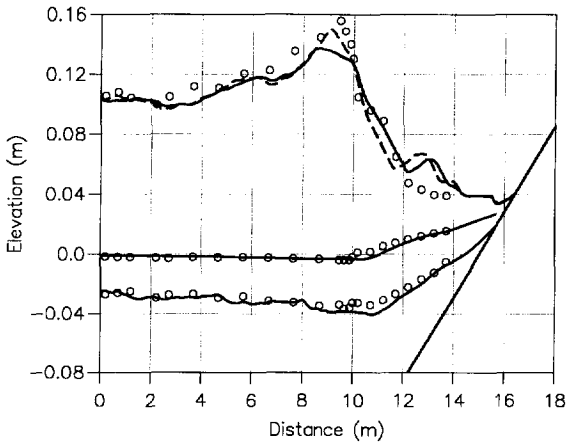

Fig. 9. Spatial variation of wave crest elevation, wave trough elevation and mean water level for the test of Ting and Kirby (1994) with plunging breakers ($T = 5$ s). Present model with default parameters (————); present model with calibrated parameters ($\phi_B = 25$ deg and $t_{1/2} = T/10$) (---); experimental data (○).

and the mean water level are in good agreement with the measurements, while the crest elevation is less satisfactory. The computed break point is approximately one meter seawards of the measured location. This may be improved by increasing ϕ_B from 20 deg to 25 deg and reducing $t_{1/2}$ from $T/5$ to $T/10$ (shown with dotted lines in Fig. 9), in which case the break point is shifted shorewards and the crest elevation follows the measurements quite closely even in the vicinity of the break point. The reason for the nonlinear shoaling being so much better compared to what was achieved in cases 1–2 is that the wavenumbers are much smaller in the present case. It is somewhat surprising to see that although the break point is shifted and the wave height at the break point is increased using $\phi_B = 25$ deg, this does not really affect the spatial variation of the trough elevation and the mean water level. The peculiar bump appearing in the crest elevation in both simulations at $x = 13$ m is caused by a secondary peak in the computed wave profile, which evolves in the surf zone due to limitations in the present breaker model.

3.2. Breaking over a submerged bar

Wave transformation over submerged bars is a challenging test case for most wave models as it involves a number of complicated processes such as nonlinear shoaling and growth of bound harmonics on the uphill slope and subsequent release of higher harmonics on the downhill slope. A successful simulation of these processes requires a model with highly accurate dispersion characteristics and nonlinear transfer properties. When wave breaking is involved in the transformation process further complications are added. Firstly, the breaking may occur on the uphill slope in which case the surf-similarity parameter is still valid as an indication of the type of breaking. Secondly, breaking may occur on the horizontal part on top of the bar, in which case it is more difficult to

define the type of breaking. A special complication in connection with the breaker model is the prediction of the position of wave breaking which is determined by the angle of incipient breaking, ϕ_B: While breaking on a plane slope will be detected sooner or later for a given value of ϕ_B, we may completely miss the breaking on the bar if ϕ_B is too large.

Luth et al. (1993) performed a series of flume experiments with regular as well as irregular waves using the bathymetry as shown in Fig. 10. Here we concentrate on a case of regular waves with a period of 1.8 s and a wave height of 0.3 m. In this case breaking occurs on the uphill slope of the bar and the type of breaking can be classified as spilling, see case 4 in Table 1. Fig. 10 shows a comparison between measurements and the computed spatial variation of the significant wave height and the mean water

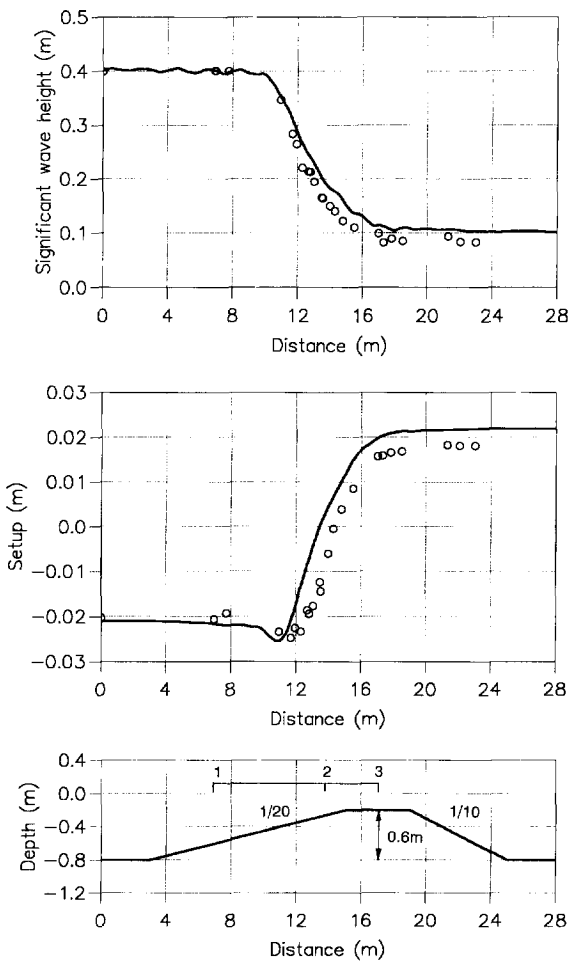

Fig. 10. Spatial variation of significant wave height (four times the standard deviation of η), the mean water level and the bathymetry for the test of Luth et al. (1993). Present model (————); experimental data (○).

level using standard breaker parameters. The wave height variation is seen to be predicted quite well but the initial decay after breaking is slightly underestimated by the model. As expected, the setup is shifted shorewards relative to the predicted break point but it is still approximately one meter off in the offshore direction in comparison to the measured setup curve. This indicates that breaking is predicted to occur somewhat too early. Relative to the still water level, the magnitude of the set-down is comparable to the set-up due to overall conservation of mass in the flume. Fig. 11 shows computed and measured timeseries of surface elevations at three locations: before the break point, in the breaking zone and after breaking. The agreement with the measurements is quite good.

Beji and Battjes (1993) used a bathymetry which was practically identical to the one used by Luth except for a scaling factor of 0.5 (see Fig. 12). Their experiments included four different tests with regular waves as listed in Table 1. In all cases breaking was rather mild and the measured break point was located either very near the end of the

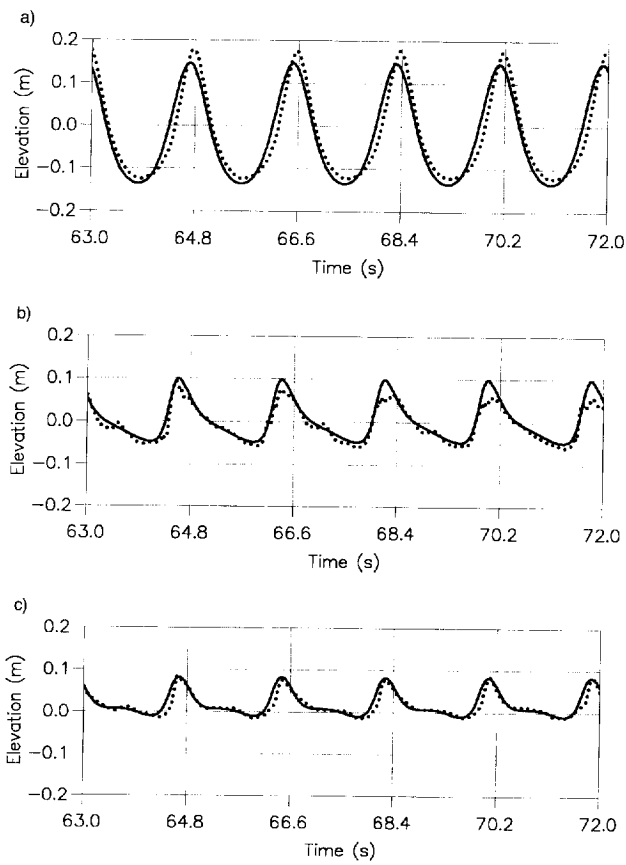

Fig. 11. Timeseries of surface elevations for the test of Luth et al. (1993). (a) Station 1, (b) station 2 and (c) station 3. Present model (————); experimental data (· · ·).

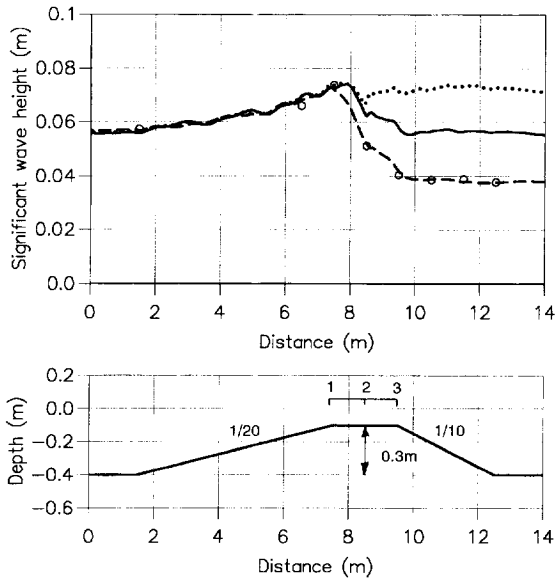

Fig. 12. Spatial variation of wave height and the bathymetry for the test of Beji and Battjes (1993). Present model with default parameters (————); present model with calibrated parameters ($\phi_B = 14$ deg and $\phi_0 = 7$ deg) (---); present model excluding breaking (· · ·); experimental data (○).

uphill slope of the bar or on the flat part on top of the bar. This makes the value of the surf-similarity parameter ζ irrelevant and consequently the classification of breaking in Table 1 is based on visual observations: Spilling breakers (s) and plunging breakers (p). With breaking occuring on top of the bar rather than on the uphill slope the test series proved to be very difficult to simulate using standard breaker model parameters: In case 6 and 8 (plunging) the energy dissipation during breaking was strongly underestimated and in case 5 and 7 (spilling) breaking was completely missed by the model. It turns out, however, that good agreement with the measurements can be obtained by reducing the breaker angles ϕ_B and ϕ_0 to approximately 14–16 deg and 7–8 deg, respectively. As an example model results from the plunging case 6 will be discussed in the following. Fig. 12 shows the spatial variation of the significant wave height computed for three different sets of model parameters: Breaking with $(\phi_B, \phi_0) = (14 \text{ deg}, 7 \text{ deg})$, breaking with standard parameters i.e. $(\phi_B, \phi_0) = (20 \text{ deg}, 10 \text{ deg})$ and finally a simulation excluding breaking. It is obvious that the first of the three simulations is superior in comparison with the measurements, while the use of standard breaker parameters leads to a clear underestimation of the dissipation. Fig. 13 shows the corresponding time series of surface elevations at three locations on top of the bar (defined in Fig. 12). The profile in station 1 is a typical nonlinear shallow water wave with higher harmonics bound to the profile. These higher harmonics are partly released between station 1 and 2 and start dominating the profile in stations 2 and 3, when breaking is not included. Using standard breaker parameters does introduce some dissipation but the overall wave shape is still very similar to the nonbreaking case. The wave profiles computed with the special set of

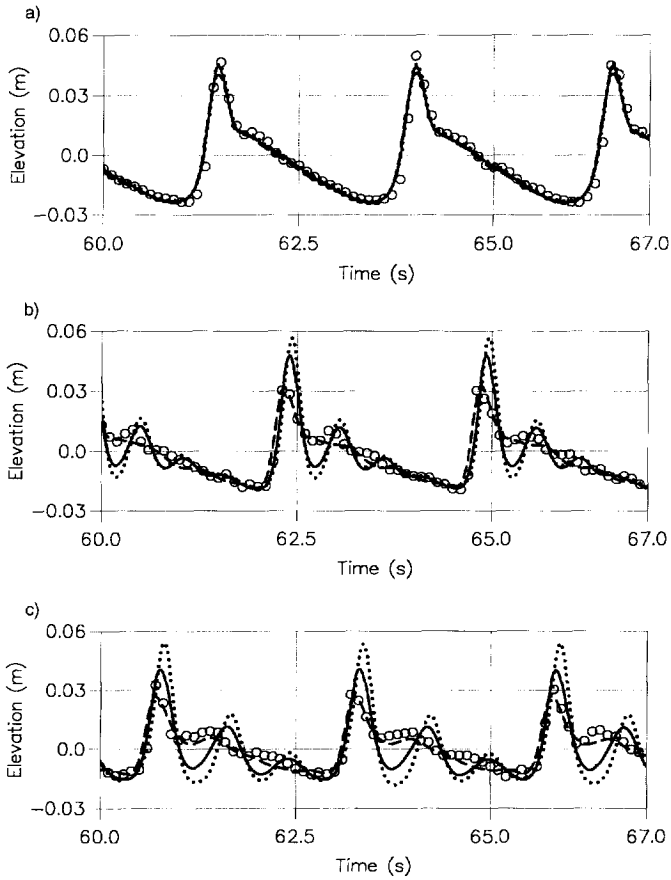

Fig. 13. Timeseries of surface elevations for the test of Beji and Battjes (1993). (a) Station 1, (b) station 2 and (c) station 3. Present model with default parameters (————); present model with calibrated parameters (ϕ_B = 14 deg and ϕ_0 = 7 deg) (– – –); present model excluding breaking (· · ·); experimental data (○).

breaker parameters i.e. (ϕ_B, ϕ_0) = (14 deg, 7 deg) are, however, significantly different from the nonbreaking case in stations 2 and 3 and the agreement with the measured profiles is very good.

3.3. Summary

From the test cases studied in the present chapter we can conclude that the breaker model with standard parameters works well for a range of different wave conditions. Although the roller model has been designed for spilling breakers on gently sloping beaches, other types of breaking may also be simulated with a moderate change of breaker angles. Plunging type of breaking appears to require a slight increase in breaker angles while breaking on top of submerged bars requires a reduction. On the other hand,

a systematic change of breaker parameters from the standard set calls for a general strategy in order to have a deterministic model and we can offer no such strategy at this moment. Fortunately, it turns out that the much more important case of breaking of irregular waves is generally less sensitive to the choice of breaker angles, and although the breaking process of irregular wave trains may easily involve spilling as well as plunging type of breaking, the variety of test cases studied in part II of this work will demonstrate that the standard set of breaker parameters is adequate for most cases.

4. Discussion of phase-averaged quantities

This chapter is devoted to an analysis and a discussion of phase-averaged momentum and energy equations consistent with the present time-domain formulation. The objective is twofold: Firstly, we want to demonstrate how the present time-domain model behaves for regular waves in a time-averaged sense. This investigation reveals the role of the individual terms in the governing equations. Secondly, the discussion will focus on important phase-averaged quantities such as the roller area, the undertow, the setup, the radiation stress, the energy flux and the energy dissipation. These quantities will in the present context be determined for regular waves by direct numerical integration over a wave period of the computed time-domain solution. These results are compared with approximative expressions used in conventional phase-averaged models (see e.g. Svendsen, 1984a,b; Dally and Brown, 1995).

The investigations in this chapter are made using the test case of Hansen and Svendsen (1984) with monochromatic spilling breakers on a plane sloping beach. This test was described in Section 3.1 and results for the wave height and setup were presented in Fig. 8. Throughout the chapter the overline notation will be used to indicate phase-averaged quantities.

4.1. The roller area and the undertow

One of the key quantities in phase-averaged models using the surface roller concept is the cross-sectional area of the roller. In line with Svendsen (1984a) and Dally and Brown (1995) we determine the roller area from the time-averaged roller thickness by using $A = c\overline{T\delta}$. In this context c is determined interactively by computing Eq. (2.6) at the steepest point of the wave front.

Fig. 14 shows the spatial variation of A computed by the Boussinesq model on the basis of the Hansen and Svendsen test treated earlier in Fig. 8. We notice that A increases gradually after the break point to a maximum value of 0.011 m^2 and then decreases towards the shoreline. The peak value of 0.011 m^2 obtained with the present model corresponds to approximately $1.0H^2$ (using the locally computed wave height), which apparently is in good agreement with Svendsen (1984a,b), who approximated the roller area by $0.9H^2$ on the basis of hydrofoil experiments by Duncan (1981). Svendsen, however, assumed an unrealistic sudden growth of A from zero to a maximum right at the break point, while a much more gradual growth was found in the experimental study by Hansen (1991) and in Dally and Brown (1995) calculations. Using digital image

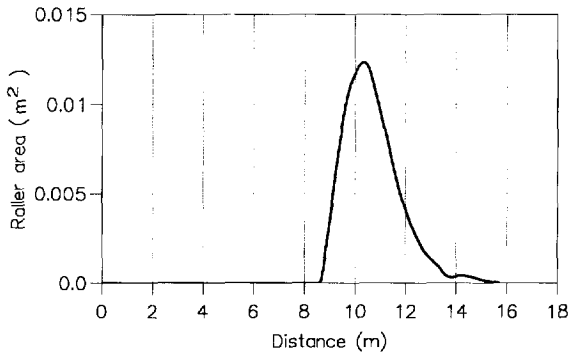

Fig. 14. Spatial variation of the roller area for case 2.

processing of video recordings of breaking waves, Hansen was able to measure not only the total aerated area, but also the part of this area which stayed at the front face of the breaking wave (the roller area). For spilling breakers with a rather small value of the surf similarity parameter, $\zeta = 0.16$, maximum values of A/H^2 were around two to three. Additional results from these experiments for a case essentially the same as the Hansen and Svendsen (1984) test exhibit values of $\max(A/H^2)$ below two and scattered around 1.5 (Hansen, 1995). Hence in comparison with these experiments Fig. 14 indicates that the roller area computed by the present model is of the right order of magnitude but a bit on the low side.

For the same data set Dally and Brown (1995) obtained a significantly larger roller area (with $\max(A/H^2) \approx 4$, see their Fig. 2). The main reason for this discrepancy is that they estimated the incoming organized energy flux by linear wave theory combined with measured wave heights at the break point. For a given wave height sinusoidal waves are far more energetic than nonlinear waves, and for this reason the actual energy flux was significantly overestimated (almost a doubling compared to the value at the offshore boundary).

The roller area is important for the return flow below the wave trough, known as the undertow. The present model allows for an estimate of the depth-averaged undertow as shown in the following. Outside the surf zone the undertow from the classical Stokes drift can be determined as, $\overline{U}$, where U is the depth-averaged velocity defined by

$$U \equiv \frac{P}{h+\eta}, \qquad P \equiv \int_{-h}^{\eta} u \, \mathrm{d}z \tag{4.1}$$

Inside the surf zone the undertow is represented by $\overline{u}_0$, where u_0 is defined by the velocity profile in Fig. 1, by which

$$u_0 = \frac{P - c\delta}{h + \eta - \delta} \tag{4.2}$$

Svendsen (1984b) approximated the time average of Eq. (4.2) by the expression

$$\overline{u_0} \approx -\frac{c}{h_{\mathrm{MWL}}^2}\left(\overline{\zeta^2} + h_{\mathrm{MWL}}\,\overline{\delta}\right), \tag{4.3}$$

where

$$\zeta \equiv \eta - \overline{\eta}, \qquad h_{\mathrm{MWL}} \equiv h + \overline{\eta} \tag{4.4}$$

The first term in Eq. (4.3) accounts for the undertow in nonbreaking waves (Stokes drift), while the additional roller effect is represented by the second term.

Fig. 15 shows the spatial variation of $\overline{U}$ and $\overline{u}_0$ computed by numerical time averaging of Eq. (4.1), Eq. (4.2) and the approximation Eq. (4.3), respectively. Again c is determined as described in Section 2.4. We notice that Eq. (4.3) is a rather crude approximation to Eq. (4.2) but that both expressions increase the magnitude of the undertow in comparison with Eq. (4.1), which ignores the roller effect. The agreement between Eq. (4.2) and the measurements of Hansen and Svendsen is relatively good. Also the NSW results of Kobayashi et al. (1989) are shown in Fig. 15, and the observed significant discrepancy with the measurements is primarily due to the large deviation in wave height (see Fig. 8) but also due to the neglect of the roller effect.

4.2. The momentum equation and the setup

In this section we shall discuss the phase-averaged momentum equation consistent with the present time domain formulation. Neglecting bottom friction, the time-average of Eq. (2.1b) in one horizontal dimension (writing ψ for ψ_x and R for R_{xx}) yields

$$\rho g h \frac{\partial \overline{\eta}}{\partial x} + \frac{\partial \overline{F}}{\partial x} + \rho \overline{\psi} + \rho \frac{\partial \overline{R}}{\partial x} = 0, \tag{4.5}$$

where ρ is the density of water and

$$\overline{F} \equiv \rho \overline{\left(\frac{P^2}{d} + \frac{1}{2} g \eta^2 \right)}. \tag{4.6}$$

Here $\overline{F}$ is the radiation stress due to the momentum from the depth averaged velocity and due to the hydrostatic part of the dynamic pressure, while $\rho\overline{\psi}$ represents the

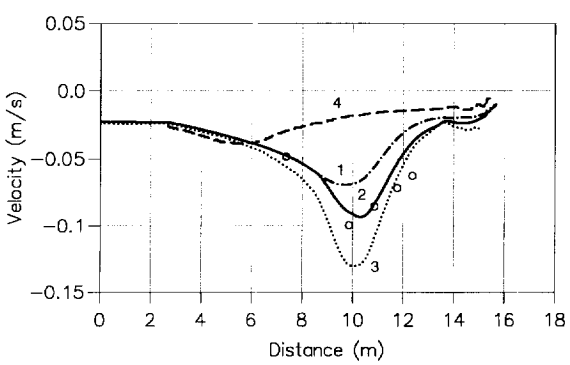

Fig. 15. Spatial variation of undertow for case 2. (1) $\overline{U}$ from Eq. (4.1); (2) $\overline{u_0}$ from Eq. (4.2); (3) $\overline{u_0}$ from the approximation Eq. (4.3); (4) numerical solution by Kobayashi et al. (1989); experimental data (○).

nonhydrostatic part of the dynamic pressure due to vertical accelerations, and $\rho\partial\overline{R}/\partial x$ is the excess momentum effect due to the nonuniform velocity distribution caused by the surface roller.

In line with Svendsen (1984a), a first estimate of $\overline{F}$ can be obtained by assuming $P \approx \sqrt{gh}\,\zeta$, which in combination with Eq. (4.4) yields

$$\overline{F} \approx \rho g\left(\tfrac{3}{2}\overline{\zeta^2} + \tfrac{1}{2}(\overline{\eta})^2\right) \tag{4.7}$$

The first term in Eq. (4.7) can be recognized as the shallow water radiation stress, which for sinusoidal waves simplifies to $3/16\rho g\mathrm{H}^2$. The second term in Eq. (4.7) represents the nonlinear part of the gravity term, which can be combined with the linear gravity term simply by replacing h by h_{MWL} in the first term of Eq. (4.5).

Fig. 16 compares the time-average of F computed using respectively Eq. (4.6), Eq. (4.7) and the sinusoidal approximation on the basis of the Boussinesq model results. It can be noticed that Eq. (4.7) is a good approximation to Eq. (4.6), while both of these estimates are clearly lower than the sinusoidal approximation. The reason is the horizontal asymmetry inherent in the computed profiles, which represent a relatively small energy for a given wave height.

The roller effect on the time-averaged momentum equation is represented by the term $\rho\partial\overline{R}/\partial x$ where $\overline{R}$ according to Eq. (2.2) can be computed by numerical time averaging of

$$R \equiv \frac{\delta}{1-\delta/d}(c-U)^2 \tag{4.8}$$

A first approximation to $\overline{R}$ is

$$\overline{R} \approx c^2\overline{\delta} \tag{4.9}$$

as used by e.g. Svendsen (1984a) and Dally and Brown (1995). Fig. 17 shows the spatial variation of $\rho\overline{R}$ determined from Eq. (4.8) and Eq. (4.9) on the basis of the model results and again c is determined interactively as described in Section 2.4. It is seen that Eq. (4.9) is a relatively poor approximation to the time-average of Eq. (4.8).

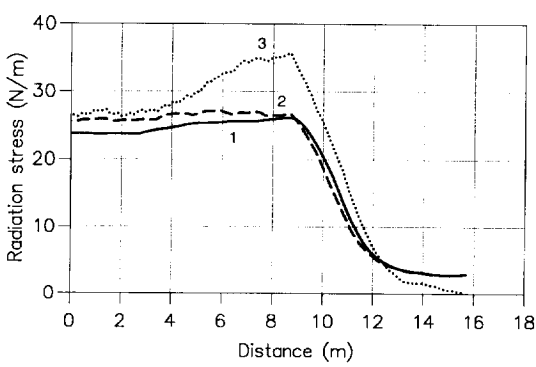

Fig. 16. Spatial variation of the radiation stress for case 2. (1) $\overline{F}$ using Eq. (4.6); (2) $\overline{F}$ using Eq. (4.7); (3) $3/16\rho gH^2$.

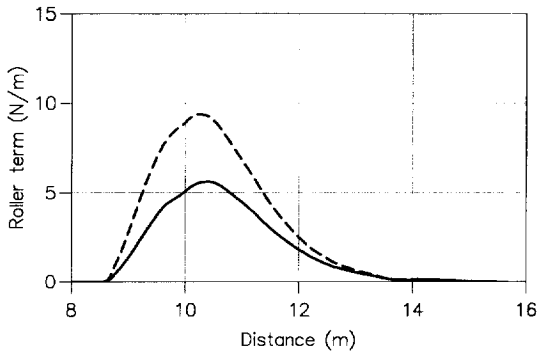

Fig. 17. Spatial variation of the roller excess momentum term $\rho\bar{R}$ for case 2. Obtained from Eq. (4.8) (————); obtained from the approximation Eq. (4.9) (---).

The computed spatial variation of the terms in the momentum balance Eq. (4.5) is shown in Fig. 18. It can be seen that $\rho\partial\bar{R}/\partial x$ gives a major contribution, and it is clearly responsible for the lateral shift between the wave height decay and the start of the setup: Instead of starting the setup at the location of $x = 8.7$ m, the setdown is actually increased initially until the setup eventually starts at the location of $x = 9.4$ m. The wave-averaged effect of the nonhydrostatic pressure $\rho\bar{\psi}$ is insignificant in this context. The sum of all terms in Eq. (4.5) is zero as expected.

4.3. The energy equation and the energy loss

In this section we focus on the phase-averaged energy equation consistent with the present time domain formulation. An obvious question to address is how the introduction of the excess roller momentum term, $\rho\partial R/\partial x$ in Eq. (2.1b) can result in dissipation

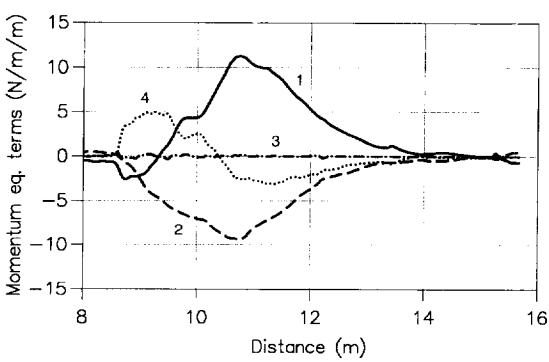

Fig. 18. Spatial variation of the terms in the wave-averaged momentum Eq. (4.5) for case 2. (1) $\rho gh\partial\bar{\eta}/\partial x$; (2) $\partial\bar{F}/\partial x$; (3) $\rho\bar{\psi}$; (4) $\rho\partial\bar{R}/\partial x$.

of the organized wave energy and how to estimate this energy loss. To answer this question we shall study the depth integrated energy equation for the wave motion i.e.

$$\frac{\partial E}{\partial t} + \frac{\partial E_F}{\partial x} + D = 0, \tag{4.10}$$

where D is the energy dissipation, and where the energy density, E and the energy flux, E_F are defined by

$$E \equiv \tfrac{1}{2}\rho g\eta^2 + \tfrac{1}{2}\rho\int_{-h}^{\eta}(u^2 + w^2)\mathrm{d}z \tag{4.11a}$$

$$E_F \equiv \int_{-h}^{\eta} u(\tilde{p} + \rho g\eta)\mathrm{d}z + \tfrac{1}{2}\rho\int_{-h}^{\eta} u(u^2 + w^2)\mathrm{d}z, \tag{4.11b}$$

with $\tilde{p}$ being the nonhydrostatic part of the dynamic pressure.

As a first estimate of the kinematics for nonbreaking shallow water waves we can express the vertical distribution of u, w and $\tilde{p}$ by

$$u(x, z, t) \approx U(x, t) \tag{4.12a}$$

$$w(x, z, t) \approx -z\frac{\partial U}{\partial x} - \frac{\partial(hU)}{\partial x} \tag{4.12b}$$

$$\tilde{p}(x, z, t) \approx \rho\left(z\frac{\partial^2(hU)}{\partial x\partial t} + \frac{z^2}{2}\frac{\partial^2 U}{\partial x\partial t}\right) \tag{4.12c}$$

which are the lowest order Boussinesq approximations satisfying local continuity and incorporating the effect of vertical accelerations. We insert Eqs. (4.12a), (4.12b) and (4.12c) in Eqs. (4.11a) and (4.11b) and obtain expressions for the energy density and energy flux. These are split up into nondispersive contributions

$$E_0 = \rho\left(\tfrac{1}{2}g\eta^2 + \tfrac{1}{2}U^2 d\right), \qquad E_{F,0} = \rho U\left(g\eta d + \tfrac{1}{2}U^2 d\right) \tag{4.13}$$

and dispersive Boussinesq type contributions,

$$E_1 \approx \rho\left(\frac{h^3}{6}\left(\frac{\partial U}{\partial x}\right)^2 + \frac{h^2}{2}U\frac{\partial U}{\partial x}\frac{\partial h}{\partial x}\right), \qquad E_{F,1} \approx -\rho U\left(\frac{h^3}{3}\frac{\partial^2 U}{\partial x\partial t} + \frac{h^2}{2}\frac{\partial U}{\partial t}\frac{\partial h}{\partial x}\right), \tag{4.14}$$

where Eq. (4.14) has been simplified by including quadratic nonlinearities only and using mild-slope approximations. On the basis of Eq. (4.13) and the depth-integrated continuity equation, we obtain the relation

$$\frac{\partial E_0}{\partial t} + \frac{\partial E_{F,0}}{\partial x} = \rho U\left(\frac{\partial}{\partial t}(Ud) + \frac{\partial}{\partial x}(U^2 d) + gd\frac{\partial \eta}{\partial x}\right) \tag{4.15}$$

while Eq. (4.14) leads to

$$\frac{\partial E_1}{\partial t} + \frac{\partial E_{F,1}}{\partial x} = \rho U\psi_1 \tag{4.16}$$

with

$$\psi_1 = -\frac{h^3}{3}\frac{\partial^3 U}{\partial x^2\partial t} - h^2\frac{\partial h}{\partial x}\frac{\partial^2 U}{\partial x\partial t} \tag{4.17}$$

We note that ψ_1 is the dispersive momentum term which can be defined in terms of the nonhydrostatic pressure as

$$\psi_1 \equiv \int_{-h}^{0} \frac{\partial \tilde{p}}{\partial x} \mathrm{d}z \tag{4.18}$$

and that Eq. (4.18) agrees with Eq. (4.17) when Eq. (4.12c) is used.

The next step is to combine Eq. (4.15) and Eq. (4.16) and time-average the result over a wave period, which yields

$$\frac{\partial \overline{E}_{\mathrm{F},0}}{\partial x} + \frac{\partial \overline{E}_{\mathrm{F},1}}{\partial x} = \rho U \overline{\left(\frac{\partial}{\partial t}(Ud) + \frac{\partial}{\partial x}(U^2 d) + gd\frac{\partial \eta}{\partial x} + \psi_1 \right)} \tag{4.19}$$

From Eq. (4.19) we conclude that the depth-integrated energy equation can be obtained simply by multiplying the depth-integrated momentum equation by the depth-averaged velocity U, followed by a time-averaging of the result.

For nonbreaking waves the actual momentum Eq. (2.1b) solved by the present model deviates from the right hand side of Eq. (4.19) in the sense that ψ defined by Eq. (2.3a) is not identical with ψ_1 given by Eq. (4.17). This indicates that the kinematics assumed in Eqs. (4.12a), (4.12b) and (4.12c) are not in full agreement with the momentum equation solved by the present model and consequently the expression Eq. (4.14) for $E_{\mathrm{F},1}$ is only a first estimate of the energy flux in the model. To investigate this discrepancy we split up ψ from Eq. (2.3a) into the two contributions

$$\begin{aligned} \psi_{\mathrm{A}} &= -\tfrac{1}{3}h^2 \frac{\partial^3 P}{\partial x^2 \partial t} - \frac{h}{3}\frac{\partial h}{\partial x}\frac{\partial^2 P}{\partial x \partial t}, \\ \psi_{\mathrm{B}} &= -Bh^2 \left(\frac{\partial^3 P}{\partial x^2 \partial t} + gh\frac{\partial^3 \eta}{\partial^3 x} + 2g\frac{\partial h}{\partial x}\frac{\partial^2 \eta}{\partial x^2} \right) \end{aligned} \tag{4.20}$$

Note that ψ_{B} represents the linear terms of higher order added to the momentum equation in order to improve the linear dispersion characteristics (Madsen and Sørensen, 1992). In theory as well as in practice ψ_{B} has little influence on the time-averaged equations in shallow water and in the surf zone. The other term, ψ_{A} simplifies to ψ_1 using the approximation $P \approx Uh$. This approximation is consistent with the neglect of higher order nonlinearities in connection with the dispersive terms, but in practice it will deviate from ψ_1 where strong nonlinearities occur. Hence, although to the lowest order in dispersion and nonlinearity the energy fluxes expressed by Eq. (4.13) and Eq. (4.14) are consistent with the equations solved by the present model, the difference between ψ_1 and ψ can not be ignored in practice, and by substituting Eq. (2.1b) without the R-term into Eq. (4.19), we get

$$\frac{\partial \overline{E}_{\mathrm{F},0}}{\partial x} + \frac{\partial \overline{E}_{\mathrm{F},1}}{\partial x} = \rho \overline{U(\psi_1 - \psi)}, \tag{4.21}$$

which is the depth-integrated and time-averaged energy equation corresponding to the present model in case of no dissipation.

When the waves are breaking the R-term will appear in the momentum equation and

repeating the above procedure i.e. multiplying the momentum equation by U followed by time-averaging leads to

$$\frac{\partial \bar{E}_{F,0}}{\partial x} + \frac{\partial \bar{E}_{F,1}}{\partial x} = \rho \overline{U(\psi_1 - \psi)} - \rho \overline{U \frac{\partial R}{\partial x}} \tag{4.22}$$

Note that Eq. (4.22) has been derived without consideration of the vertical distribution of the horizontal velocity (Fig. 1) although this is exactly what is causing the R-term in the first place. If such vertical details are taken into account in the formal derivation of the energy and the energy flux, an alternative energy equation will appear as we shall see later in this section. Here we emphasize, however, that the objective is to estimate the dissipative effect of the R-term occuring in the depth-integrated momentum equation. From that point of view vertical details are irrelevant as terms are formulated in bulk quantities such as the surface elevation and the depth-averaged velocity. The last term in Eq. (4.22) appears only in connection with wave breaking, hence it is natural to interpret this term as the effective energy dissipation occuring in the model i.e.

$$\overline{D_1} = \rho \overline{U \frac{\partial R}{\partial x}} \tag{4.23}$$

Fig. 19 shows the computed spatial variation of the terms in the energy balance Eq. (4.22). First of all it is seen that the sum of the terms is practically zero everywhere, which needs to be checked, since Eq. (4.22) is actually not solved by the numerical model. We notice that $\rho \overline{U \partial R / \partial x}$ obviously plays an important role in the surf zone and that it basically burns off the amount of energy flux from the seaward boundary.

Fig. 20 shows the computed spatial variation of the time-averaged energy fluxes, where $E_{F,0}$ is split into the two contributions given by Eq. (4.13). As expected, the contribution from the hydrostatic part of the dynamic pressure is generally dominating, while the cubic velocity term is rather small. The effect of the nonhydrostatic part of the dynamic pressure represented by the time-average of $E_{F,1}$ from Eq. (4.14) is always counteracting the hydrostatic part and it is typically 10% of its magnitude.

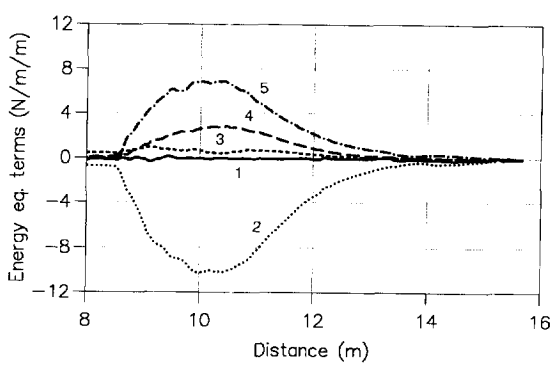

Fig. 19. Spatial variation of the terms in the time-averaged energy equation Eq. (4.22) for case 2. (1) sum of all terms, (2) $\partial(\bar{E}_{F,0})/\partial x$; (3) $\partial(\bar{E}_{F,1})/\partial x$; (4) $\rho \overline{U(\psi - \psi_1)}$; (5) $\rho \overline{U \partial R / \partial x}$.

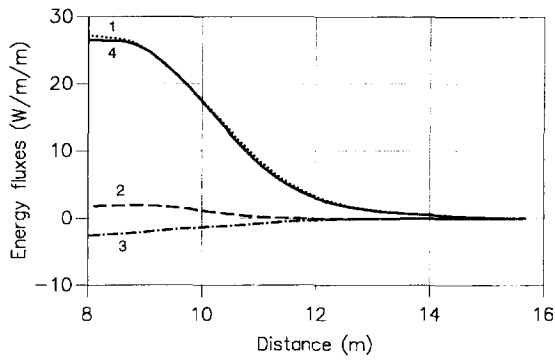

Fig. 20. Spatial variation of the time-averaged energy fluxes for case 2. (1) $\rho g\overline{\eta U d}$; (2) $\rho/2\overline{U^3 d}$; (3) $\overline{E}_{F,1}$; (4) $\overline{E}_{F,0} + \overline{E}_{F,1}$.

In general the use of phase-averaged models involves an explicit formulation of the energy loss $\overline{D}$ and a common model from the literature is based on the classical hydraulic jump analogy (see e.g. Svendsen et al., 1978; Svendsen, 1984a). More recently Deigaard (1989) used the roller concept and estimated the energy dissipation as the product of the local roller pressure gradient and the horizontal flow velocity, while Dally and Brown (1995) estimated the dissipation by the friction at the interface between the roller and the underlying flow. In both cases the energy dissipation due to the roller was formulated as

$$\overline{D_2} = \rho g c \overline{\delta} \beta_D, \tag{4.24}$$

where β_D is a function of the angle of inclination of the roller and proportional to the angle if this is small. While Deigaard suggested to use the value $\beta_D = 0.18$ (corresponding to a fixed roller angle of 10 degrees), Dally and Brown calibrated their model with $\beta_D = 0.10$. We have computed the spatial variation of Eq. (4.24) with $\beta_D = 0.10$ by using the Boussinesq model results for $\overline{\delta}$ and c (determined interactively). Fig. 21 shows a comparison between $\overline{D_2}$ from Eq. (4.24) and $\overline{D_1}$ from Eq. (4.23), representing the actual energy loss occuring in the simulation. The agreement is quite good and gives some support to the value of $\beta_D = 0.10$.

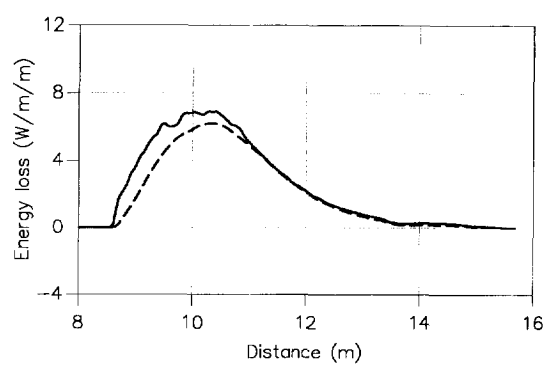

Fig. 21. Spatial variation of the energy loss for case 2. $\rho\overline{U\partial R/\partial x}$ (————); 0.1 $\rho g c \overline{\delta}$ (---).

Finally we shall return to the formal derivation of the energy and the energy flux taking the vertical details of the velocity profile in Fig. 1 into account and deriving an energy equation from Eq. (4.10) without directly involving the momentum equation. For simplicity we shall assume that w and $\tilde{p}$ can still be approximated by Eqs. (4.12a), (4.12b) and (4.12c). In addition to (E_0, $E_{F,0}$) and (E_1, $E_{F,1}$) given by Eq. (4.13) and Eq. (4.14) this leads to the following excess energy density (E_2) and excess energy flux ($E_{F,2}$) due to the surface roller

$$E_2 = \tfrac{1}{2}\rho\left(c^2\delta + u_0^2(d-\delta) - U^2 d\right), \qquad E_{F,2} = \tfrac{1}{2}\rho\left(c^3\delta + u_0^3(d-\delta) - U^3 d\right) \tag{4.25}$$

and the resulting time-averaged energy equation reads

$$\frac{\partial}{\partial x}\left(\overline{E}_{F,0} + \overline{E}_{F,1} + \overline{E}_{F,2}\right) + \overline{D} = 0, \tag{4.26}$$

which is similar to the equation considered by Svendsen (1984a) and Dally and Brown (1995). Note that in Eq. (4.26) $\overline{D}$ has to be modelled explicitly e.g. by the use of Eq. (4.24). The role of $\overline{E}_{F,2}$ in Eq. (4.26) is mainly a redistribution of the energy loss somewhat similar to the redistribution of the setup in the time-averaged momentum equation.

If the intention is to incorporate an independent energy equation in the system of model equations, Eq. (4.26) is a logical consequence of the velocity profile introduced in Fig. 1. However, with the present phase-resolving Boussinesq model combined with the breaker model described in Section 2 there is no need of an independent energy equation like Eq. (4.26) and the model has no inherent information about it. Instead Eq. (4.22) derived directly from the momentum equation is the relevant energy equation in this context.

5. Conclusion

A phase-resolving numerical model for waves and wave-driven currents in and near the surf zone is presented. The nondissipative part of the model is of Boussinesq type and it includes improved dispersion properties relative to the classical Boussinesq equations. The dissipative part is based on a surface roller concept for spilling breakers. The instantaneous determination of the surface roller is based on a simple heuristic approach. The roller gives rise to additional convective terms in the depth-integrated momentum equations leading to a loss of energy. The shoreward boundary condition allows for a moving shoreline thus including the swash zone. The model is formulated in two horizontal dimensions.

In this paper (part I) we concentrate on cross-shore motion of regular waves with emphasis on how the time-domain model behaves in a phase-averaged sense. We analyze the mechanisms of the roller model by computing the balance in the mass, momentum and energy averaged over a wave period. In this connection important phase-averaged quantities such as the roller area, the undertow, the setup, the radiation

stress, the energy flux and the energy dissipation are computed by numerical time-averaging and the role of the individual terms in the governing equations is discussed and illustrated. The following conclusions are made: Firstly, the inclusion in the mass balance of the net mass transport due to the roller has a significant effect on the time-average of the depth-averaged particle velocities and it improves significantly the prediction of the depth-averaged undertow in the surf zone. Secondly, the inclusion in the momentum balance of additional convective terms due to the roller, leads to the well known shift between the break point and the point where the setup in the mean water level is initiated. Hence due to the presence of these additional terms the radiation stress may keep constant for a while, even though the wave height starts to decay. Thirdly, we address the question of how the introduction of the excess roller momentum term can result in energy dissipation and wave height decay. It is demonstrated that the effective energy dissipation occuring in the model should be determined as the time average of the roller momentum term multiplied by the depth averaged velocity. In the literature a more sophisticated phase-averaged energy equation is often applied including the excess roller energy flux and an explicit expression for the dissipation. We conclude that such an equation is irrelevant in the present context although it is a logical consequence of the velocity profile used.

In order to establish the relation to traditional phase-averaged formulations we compare the radiation stress, the roller momentum and the energy dissipation computed by the present model with various approximative expressions from the literature: Our computations confirm that a simple approximation of the radiation stress in terms of the surface elevation alone is quite good while an approximation using sinusoidal theory gives a significant overestimation. The excess momentum flux due to the surface roller is found to be significantly overestimated by the approximation commonly used in phase-averaged models. Two expressions from the literature suggest that the local time-averaged dissipation is proportional to the product of the celerity and the mean roller thickness. Our example supports this formulation favouring the factor of proportionality proposed by Dally and Brown (1995).

The present phase-resolving model is verified on a number of test cases involving regular waves breaking on a plane sloping beach or over a bar profile. The determination of the surface roller relies on four parameters. A sensitivity analysis indicates that for a number of cases the choice of these parameters is not very critical. A standard set of parameters is chosen, and with this set the model can be used as a predictive tool. All results are shown using the standard parameter set and in the few cases where the results are less satisfactory, it is shown how the adjustment of these parameters could better the agreement with measurements. All cases calling for adjustment of the parameter set were known a priori to be difficult examples: This is either due to plunging type wave breaking, while the present model is developed for spilling breakers, or to breaking occuring on the flat top of a bar, which (to our knowledge) no other model can simulate to satisfaction without calibration.

The examples of cross-shore motion of regular waves tend to illuminate the weaknesses rather than the strengths of the present model, and many calibrated phase-averaged models can most likely perform equally well (if not better) on these relatively simple cases. The real strength of the present model lies in its flexibility, which makes it

possible to automatically capture the (time-varying) point of incipient breaking as well as cessation of breaking. This allows for the simulation of wave breaking and run-up of irregular, multidirectional waves in two horizontal dimensions and a study of phenomena like swash oscillations and surf beats induced by short-wave groups as well as rip currents and nearshore circulations. Such applications are presented in part II and III of this work.

Acknowledgements

This work was financed by the Danish National Research Foundation and their support is greatly appreciated. Many thanks are due to Jürjen Battjes, Yasser Eldeberky and Marteen Dingemans, who kindly provided experimental data for some of the test cases. Rolf Deigaard and Karim Rakha also influenced the work in this paper and finally we thank Buhr Hansen for providing some unpublished data and Bill Dally for sending his manuscript before publication.

References

Abbott, M.B., Larsen, J., Madsen, P.A., Tao, J., 1983. Simulation of wave breaking and run-up. In Seminar on Hydrodynamics of waves in coastal areas. 20th Congr. of IAHR. IAHR, Moscow.

Beji, S., Battjes, J.A., 1993. Experimental investigations of wave propagation over a bar. Coastal Eng. 19, 151–162.

Battjes, J.A., 1974. Surf Similarity. In: Proc. of the 14th Coastal Eng. Conf. ASCE, pp. 466–480.

Battjes, J.A., 1988. Surf-zone dynamics. Annu. Rev. Fluid Mech. 20, 257–293.

Brocchini, M., Drago, M., Iovenitti L., 1992. The modelling of short waves in shallow waters: Comparison of numerical models based on Boussinesq and Serre equations. In: Proc. of the 23th Coastal Eng. Conf., ch. 4, pp. 76–89.

Carrier, G.F., Greenspan, H.P., 1958. Water waves of finite amplitude on a sloping beach. J. Fluid Mech. 4, 97–109.

Dally, W.R., Brown, C.A., 1995. A modeling investigation of the breaking wave roller with application to cross-shore currents. J. Geophys. Res. 100 (C12), 24873–24883.

Deigaard, R., 1989. Mathematical modelling of waves in the surf zone. Prog. Rep. 69. ISVA, Technical University, Lyngby, pp. 47–59.

Duncan, J.H., 1981. An experimental investigation of breaking waves produced by a towed hydrofoil. Proc. R. Soc. London Ser. A 377, 331–348.

Eldeberky, Y., Battjes, J.A., 1996. Spectral modelling of wave breaking: Application to Boussinesq equations. J. Geophys. Res. 102, 1253–1264.

Elgar, S., Freilich, M.H., Guza, R.T., 1990. Model-data comparisons of moments of non breaking shoaling surface gravity waves. J. Geophys. Res. 95 (C9), 16055–16065.

Freilich, M.H., Guza, R.T., 1984. Nonlinear effects on shoaling surface gravity waves. Philos. Trans. R. Soc. London A311, 1–41.

Galvin, C.J. Jr., 1968. Breaker type classification on three laboratory beaches. J. Geophys. Res. 73 (12), 3651–3659.

Hamm, L., Madsen, P.A., Peregrine, D.H., 1993. Wave transformation in the nearshore zone: A review. Coastal Eng. 21, 5–39.

Hansen, J.B., Svendsen, I.A., 1984. A theoretical and experimental study of undertow. Proc. of the 19th Coastal Eng. Conf., pp. 2246–2262.

Hansen, J.B., 1991. Air entrainment in surf zone waves, Proc. Copedec, Mombassa, pp. 1357–1371.

Hansen, J.B., 1995. Private communication.
Hibberd, S., Peregrine, D.H., 1979. Surf and run-up on a beach: A uniform bore. J. Fluid Mech. 95 (Part 2), 323–345.
Kaihatu, J.M., Kirby, J.T., 1995. Nonlinear transformation of waves in finite water depth. Phys. Fluids 7, 1903–1914.
Karambas, Th., Koutitas, C., 1992. A breaking wave propagation model based on the Boussinesq equations. Coastal Eng. 18, 1–19.
Kobayashi, N., De Silva, G.S., Watson, K.D., 1989. Wave transformation and swash oscillation on gentle and steep slopes. J. Geophys. Res. 94 (C1), 951–966.
Larsen, J., Dancy, M., 1983. Open boundaries in short wave simulations: A new approach. Coastal Eng. 7, 285–297.
Lippmann, T.C., Brookins, A.H., Thornton, E.B., 1996. Wave energy transformation on natural profiles. Coastal Eng. 27, 1–20.
Luth, H.R., Klopman, G., Kitou, N., 1993. Kinematics of waves breaking partially on an offshore bar, Report H1573, Delft Hydraulics.
Madsen. P.A., Sørensen, O.R., 1992. A new form of the Boussinesq equations with improved linear dispersion characteristics. Part 2. A slowly-varying bathymetry. Coastal Eng. 18, 183–204.
Madsen, P.A., Sørensen, O.R., 1993. Bound waves and triad interactions in shallow water. Ocean Eng. 20, 359–388.
Madsen, P.A., Sørensen, O.R., Schäffer, H.A., 1997. Surf zone dynamics simulated by a Boussinesq type model. Part II. Surf beat and swash oscillations for wave groups and irregular waves. Coastal Eng. 32, 289–320.
Madsen, P.A., Schäffer, H.A., 1997. Higher order Boussinesq-type equations for surface gravity waves: Derivation and analysis. Submitted.
Mase, H., Kirby, J.T., 1992. Hybrid frequency-domain KdV equation for random wave transformation. in Proc. 23rd Int. Conf. on Coastal Engineering, Venice, pp. 474–487.
Peregrine, D.M., 1967. Long waves on a beach, J. Fluid Mech., vol. 27, Part 4.
Sato, S., Kabiling, M.B., Suzuki, H., 1991. Prediction of near-bottom velocity history by a nonlinear dispersive wave model. Coastal Eng. Jpn. 35 (1), 67–82.
Schäffer, H.A., Madsen, P.A., Deigaard, R., 1993. A Boussinesq model for waves breaking in shallow water. Coastal Eng. 20, 185–202.
Stive, M.J.F., 1980. Velocity and pressure field of spilling breakers. Proc. of the 17th Coastal Eng. Conf., pp. 547-566.
Stive, M.J.F., 1984. Energy dissipation in waves breaking on gentle slopes. Coastal Eng. 8, 99–127.
Svendsen, I.A., Madsen, P.A., Hansen J.B., 1978. Wave characteristics in the surf zone. In: Proc. 16th Coastal Eng. Conf., Hamburg, vol. I, pp. 520–539.
Svendsen, I.A., 1984a. Wave heights and setup in a surf zone. Coastal Eng. 8, 303–329.
Svendsen, I.A., 1984b. Mass flux and undertow in a surf zone. Coastal Eng. 8, 347–365.
Svendsen, I.A., Schäffer, H.A., Hansen, J.B., 1987. The interaction between the undertow and the boundary layer flow on a beach. J. Geophys. Res. 92 (c11), 845–856.
Sørensen, O.R., Schäffer, H.A., Madsen, P.A., 1998. Surf Zone Dynamics Simulated by a Boussinesq type model. Part III. Wave induced horizontal nearshore circulations. Coastal Eng., submitted.
Tao, J., 1983. Computation of wave run-up and wave breaking. Internal Report, Danish Hydraulic Institute, 40 pp.
Ting, F.C.K., Kirby, J.T., 1994. Observation of undertow and turbulence in a laboratory surf zone. Coastal Eng. 24, 51–80.
Watson, G., Peregrine, D.H., 1992. Low frequency waves in the surf zone. In Proc. of the 23th Coastal Eng. Conf., ch. 61, pp. 818–831.